



Journal homepage: <http://civiljournal.semnan.ac.ir/>

The Relationship between Compressive Strength and Splitting Tensile Strength of high-Performance Fiber-Reinforced Cementitious Composites

Mahdiah Sabbaghian¹ ; Ali Kheyroddin^{2,*} 

1. Department of Civil and Environmental Engineering, Amir Kabir University of Technology, Tehran Polytechnic, Tehran, Iran

2. Distinguished Professor, Faculty of Civil Engineering, Semnan University, Semnan, Iran

* Corresponding author: kheyroddin@semnan.ac.ir

ARTICLE INFO

Article history:

Received: 21 June 2022

Revised: 20 August 2022

Accepted: 06 December 2022

Keywords:

High-performance fiber-reinforced cement composite; HPFRCC; Compressive strength; Splitting tensile strength; Non-linear regression (NLR).

ABSTRACT

The HPFRCC is defined by a stress-strain response in tension, which demonstrates multiple cracking and strain-hardening behavior. This experimental study aims to investigate the splitting tensile strength (STS), compressive strength (CS), and bulk density (BD) of HPFRCC. The CS of concrete should provide an accurate basis for the STS prediction. This study consists of two phases; in the first phase, 18 HPFRCC mix proportions with 1% steel fibers (30 mm length) were formulated by taking into account the various types of aggregate distribution, water-to-cement (w/c) ratio, amount of superplasticizer, and silica fume. After testing 108 cylinder and cube specimens at 7 and 28 days, a mathematical exponential function between STS and CS was proposed with a prediction error of less than $\pm 15\%$. In the second phase, in order to evaluate the effect of steel fiber volume fraction and age on the prediction equation, three distinct volume fractions of steel fibers were considered: 0%, 1%, and 2%. At the ages of 7, 28, 56, and 90 days, 144 cube and cylinder specimens were tested. The proposed equation for HPFRCC with 1% steel fiber can be applied to specimens containing 2% fiber with an error of $\pm 20\%$. Adding fibers to the cementitious mortar had a small effect on the CS. However, at 28 days, the STS for HPFRCC with 1% and 2% fibers increased by 54% and 95%, respectively, compared to specimens without fibers.

1. Introduction

Concrete is one of the most often utilized building materials in the world. The

availability of constituents and concrete's high compressive strength contribute to its widespread acceptance from an economic standpoint. Despite this preponderance,

How to cite this article:

Sabbaghian, M., & Kheyroddin, A. (2023). The Relationship between Compressive Strength and Splitting Tensile Strength of high-Performance Fiber-Reinforced Cementitious Composites. *Journal of Rehabilitation in Civil Engineering*, 11(4), 1-21. <https://doi.org/10.22075/jrce.2022.27187.1667>

brittleness or low tensile strength and low resistance to cracking propagation can be considered drawbacks of concrete. High-Strength Concrete (HSC) and High-Performance Concrete (HPC) are new types of concrete being developed to meet various needs, including improving durability and mechanical properties. Moreover, the incorporation of fibers plays a crucial role in addressing these deficiencies. The concept of enhancing tensile strength and flexibility has been pondered and implemented in numerous structural engineering contexts. Steel fibers are one of the many types of fibers currently added to concrete for various applications [1]. Steel fibers have high elastic modulus and fracture strain, making them one of the most appropriate and cost-effective fibers due to their acceptable ductility and high tensile strength. Cementitious composites are concrete composed solely of fine aggregates, including mortar and fibers. Mortar is made from aggregates, cementitious material, and superplasticizers. Fiber also controls the opening and expansion of cracks [2]. High-Performance Fiber-Reinforced Cementitious Composites (HPFRCC) are characterized by a stress-strain response in tension, which demonstrates multiple cracking behaviors, strain-hardening behavior, and relatively large energy absorption capacity. In previous publications, several researchers have addressed the use of steel fibers in concrete and cementitious composites [3–12]. Recent studies have introduced the application of machine learning techniques to identify the governing relationships in material behavior. Previous research has demonstrated that the type of steel fibers and aggregates are primarily affected by both the tensile strengths (TS) and the compressive strength (CS) of concrete [13,14]. Among other

parameters, predictions of concrete's splitting tensile strength (STS) are remarkable. Concrete's CS should provide an accurate basis for STS prediction. Numerous equations have been proposed for STS-CS relationships, with Eq.1 being the most widely accepted [15–18].

$$f_{sp} = \alpha \times (fc')^\beta \quad (1)$$

Where f_{sp} is STS (MPa); fc' is the specified CS (MPa); α and β are regression coefficients. So far, researchers investigating the correlation between STS and CS in fiber concrete have provided scant empirical evidence. Nataraja et al. suggested a linear relationship between CS and TS for SFRC with normal strength [16]. Several exponential mathematical functions were proposed for STS prediction, with different values of α and β given by different researchers, as shown in Table 1.

The primary target of this empirical study is to investigate the mechanical properties of the HPFRCC material with steel fibers. Variable steel fiber volume fractions, w/b ratios, silica fume, fourteen different aggregate distributions (consisting of quartz, natural and crushed sand), and ages were used to produce the HPFRCC series. The primary objective was to establish the STS, CS, and BD of HPFRCC. Also, this study aimed to demonstrate the relationship between STS and CS. This article contains two sections; First, an exponential function was proposed to predict the STS basis of CS for HPFRCCs with 1% steel fibers, and second, the effect of age and steel volume fraction on the previous equations was investigated. Fig. 1 demonstrates the flowchart of the experimental program.

Table 1. The relationship between STS and CS of concrete.

| Code of practice/ researcher | Empirical relation | Comments |
|---------------------------------|--------------------------------------|--|
| ACI-363R-92 [19] | $f_{sp} = 0.59f_c^{0.5}$ | $21 < f_c < 83$ MPa |
| ACI-318-95 [20] | $f_{sp} = 0.56f_c^{0.5}$ | - |
| Ahmed and Shah [15] | $f_{sp} = 0.46f_c^{0.55}$ | $15 < f_c < 84$ MPa |
| Raphael [21] | $f_{sp} = 0.31f_c^{0.67}$ | Normal concrete; for $f_c < 40$ MPa |
| Nilson [22] | $f_{sp} = 0.62f_c^{0.5}$ | - |
| Wafa and Ashour [23] | $f_{sp} = 0.58f_c^{0.5}$ | Steel fiber reinforced concrete |
| Xu and Shi [18] | $f_{sp} = 0.21f_c^{0.83}$ | Steel fiber reinforced concrete |
| Zaint et al.[24] | $f_{sp} = \frac{f_c}{0.1f_c + 7.11}$ | High-performance concrete $f_c > 40$ Mpa |
| Ramadoss et al [25] | $f_{sp} = 0.188f_c^{0.84}$ | high-performance steel fiber–reinforced concrete |
| Gardner et al. [26] | $f_{sp} = 0.46f_c^{0.6}$ | $13 < f_c < 72$ MPa; Type III cement concretes |

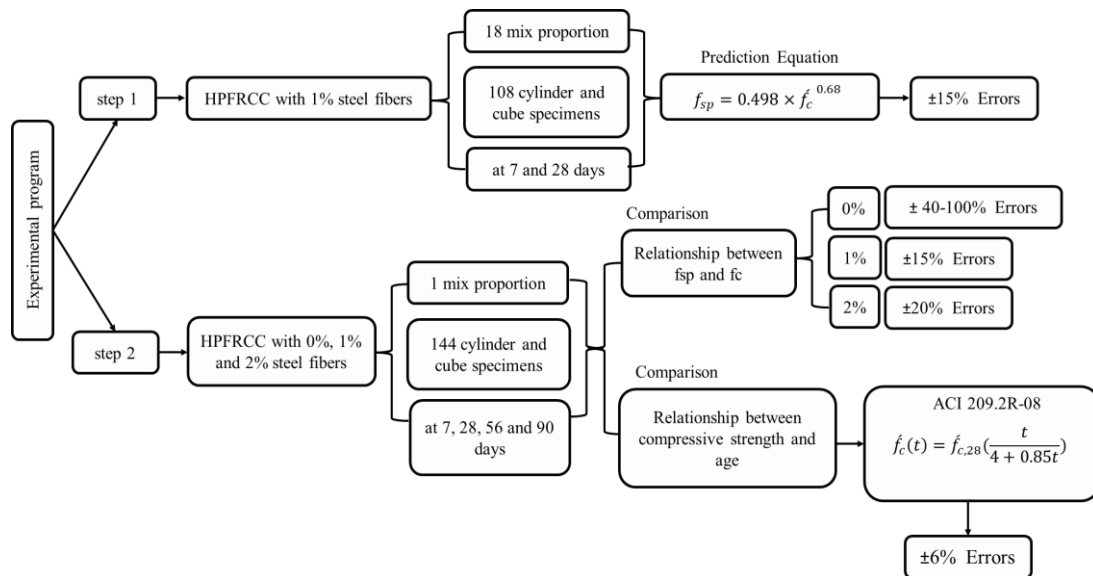


Fig. 1. Flowchart of the experimental program.

2. Experimental program

This study consists of two phases; in the first phase, 18 mix proportions of HPFRCC were created, and 108 cylinder and cube specimens of HPFRCC were tested at 7, 28 days. Furthermore, the relationship between HPFRCC's CS and STS was predicted. In the second step, the effect of steel fiber fraction volume and age on the prediction equation was evaluated by considering three different

steel fiber volume fractions: 0%, 1%, and 2%. At 7, 28, 56, and 90 days, 144 cube and cylinder specimens were tested.

2.1. Material

As cementitious materials, all concrete mixtures contained type II Portland cement and silica fume (0.05-0.015m). Table 2 displays the chemical composition of cement and silica fume.

Table 2. Chemical composition of used cement and silica fume.

| Chemical formula | Cement type II | Silica fume |
|------------------------------------|----------------|-------------|
| SiO ₂ (%) | 21.4 | 94 |
| Al ₂ O ₃ (%) | 4.5 | 1.1 |
| Fe ₂ O ₃ (%) | 4.07 | 1.1 |
| CaO (%) | 63.6 | 0.11 |
| MgO (%) | 1.54 | 0.14 |
| SO ₃ (%) | 2.35 | 0.28 |
| Na ₂ O (%) | 0.37 | 0.29 |
| K ₂ O (%) | 0.55 | 0.25 |
| CaO.f (%) | 1.23 | - |
| Cl | - | 0.2 |
| LO.I (%) | 2.42 | 2.61 |
| Insoluble residue (%) | 0.32 | - |
| C ₃ S (%) | 49.5 | - |
| C ₂ S (%) | 24.6 | - |
| C ₃ A (%) | 5.1 | - |
| C ₄ AF (%) | 12.5 | - |

The aggregate skeleton of HPFRCC was composed of quartz sand (labeled T181 and T141), natural sand, and crushed sand, the physical properties of which are detailed in Table 3. According to ASTM C494 [27], type F superplasticizer PX-MIX is a polymer product based on polycarboxylate ether with PH 5-6; it was used in the amount of 0.8 weight of cementitious materials. As shown in Fig. 2, the HPFRCC material was reinforced with hooked steel microfibers. The properties of hooked steel microfibers are listed in Table 3, as reported by ASTM A820 [28].

Table 3. physical characteristics of aggregates.





| | T181 Quartz sand | T141 Quartz sand | natural sand | crushed sand |
|---------------------|---|---|--|---|
| specific gravity | 2.6 | 2.67 | 2.64 | 2.63 |
| water absorption | 0.93 | 1.06 | 2.7 | 3.1 |
| aggregate size | 0.09-0.35 mm | 0.18-0.71 mm | 0-4.75 mm | 0-4.75 mm |
| Modulus of softness | 0.7 | 2.4 | 4.19 | 4 |
| Picture |  |  |  |  |

Table 4. Properties of Hooked steel fiber.

| Aspect ratio | Tensile strength (MPa) | Density (kg/m ³) | Length (mm) | diameter (mm) | modulus of elasticity (GPa) |
|--------------|------------------------|------------------------------|-------------|---------------|-----------------------------|
| 37.5 | 1050 | 7850 | 30 | 8 | 200 |

**Fig. 2.** Hooked steel fiber [4].

2.2. HPFRCC Mix

The details of 21 HPFRCC mix proportions with an extremely low water-to-binder (w/b) ratio are provided in Table 5. The five variables are the amount of cement at 580 and 650 $\frac{\text{kg}}{\text{m}^3}$, the amount of silica fume at 68 and 177 $\frac{\text{kg}}{\text{m}^3}$, the volume fraction of steel fibers at 0%, 1%, and 2%, the superplasticizer content at 0.8%, 1%, 1.1%, 1.2% and 1.8% by mass, and the w/b ratio between 0.19 and 0.3 by mass. All mixes were formulated according to the ACI 544-1R [27]. The mixing procedure (Fig.3-a) was as follows: first, cement, silica fume, and aggregates were dry premixed; then, 75% of water was poured into the dry mixture; and

finally, the superplasticizer with residual water was added to the mixture after the dry mixture had been premixed. After adding superplasticizer and water, the HPFRCC mixture became fluid within 5-7 minutes. During the following 5 to 7 minutes, fibers scattered. The mortar flow test was conducted in accordance with ASTM C143 [29], with an average slump of 70mm (Fig.3-b). Freshly mixed HPFRCC was cast into the cube and cylindrical molds (Fig.3-c) and removed from the molds 24 hours later in a laboratory with a temperature of $20 \pm 2^\circ\text{C}$. In accordance with ASTM C31[30], HPFRCC specimens were cured by submersion in water (Fig.3-d) for 28 days at a temperature of $23 \pm 2^\circ\text{C}$.



Fig. 3. a) The mixing procedure. b) the slump tests. c) casting. d) curing of HPFRCC specimens.

Table 5. Mix design of HPFRCC (data for 1 m³).

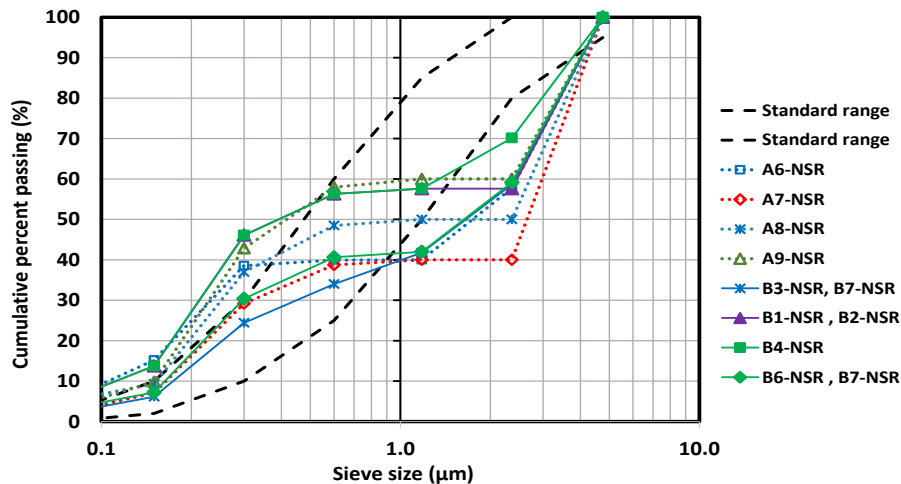
| Step | Design parameters | | | | | Mix proportion (kg/m ³) | | | | | | |
|------|-------------------|-----------------|------|------|------|-------------------------------------|--------|----------------|---|--------|--------|--------|
| | No | Mix designation | w/b | w*/c | w/c | A (kg) | SP (%) | V _f | | W (kg) | M (kg) | C (kg) |
| | | | | | | | | (kg) | % | | | |
| One | 1 | A1-SR | 0.3 | 0.34 | 0.34 | 1480 | 0.8 | 78.5 | 1 | 194 | 68 | 580 |
| | 2 | A2--SR | 0.3 | 0.34 | 0.34 | 1480 | 0.8 | 78.5 | 1 | 194 | 68 | 580 |
| | 3 | A3-SR | 0.24 | 0.29 | 0.27 | 1570 | 1.8 | 78.5 | 1 | 154 | 68 | 580 |
| | 4 | A4-SR | 0.3 | 0.34 | 0.34 | 1460 | 0.8 | 78.5 | 1 | 194 | 68 | 580 |
| | 5 | A5-SR | 0.3 | 0.34 | 0.34 | 1460 | 0.8 | 78.5 | 1 | 194 | 68 | 580 |
| | 6 | A6-NSR | 0.28 | 0.32 | 0.31 | 1470 | 0.8 | 78.5 | 1 | 181 | 68 | 580 |
| | 7 | A7-NSR | 0.29 | 0.33 | 0.32 | 1470 | 0.8 | 78.5 | 1 | 188 | 68 | 580 |
| | 8 | A8-NSR | 0.29 | 0.33 | 0.32 | 1470 | 0.8 | 78.5 | 1 | 188 | 68 | 580 |
| | 9 | A9-NSR | 0.29 | 0.33 | 0.32 | 1470 | 0.8 | 78.5 | 1 | 188 | 68 | 580 |
| | 10 | B1-NSR | 0.19 | 0.27 | 0.24 | 1326 | 1.8 | 78.5 | 1 | 158 | 177 | 650 |
| | 11 | B2-NSR | 0.22 | 0.3 | 0.28 | 1263 | 1.8 | 78.5 | 1 | 182 | 177 | 650 |
| | 12 | B3-NSR | 0.29 | 0.38 | 0.37 | 1158 | 0.8 | 78.5 | 1 | 240 | 177 | 650 |
| | 13 | B4-NSR | 0.19 | 0.27 | 0.24 | 1325 | 1.8 | 78.5 | 1 | 158 | 177 | 650 |
| | 14 | B5-NSR | 0.24 | 0.32 | 0.31 | 1253 | 1.2 | 78.5 | 1 | 198 | 177 | 650 |
| | 15 | B6-NSR | 0.27 | 0.35 | 0.34 | 1197 | 0.8 | 78.5 | 1 | 223 | 177 | 650 |
| | 16 | B7-NSR | 0.23 | 0.31 | 0.29 | 1285 | 1 | 78.5 | 1 | 190 | 177 | 650 |
| | 17 | B8-SR | 0.23 | 0.31 | 0.29 | 1284 | 1.1 | 78.5 | 1 | 190 | 177 | 650 |
| | 18 | B9-SR | 0.29 | 0.38 | 0.37 | 1149 | 1.2 | 78.5 | 1 | 240 | 177 | 650 |
| Two | 19 | HPCC | 0.3 | 0.34 | 0.34 | 1420 | 0.8 | 0 | 0 | 198 | 68 | 580 |
| | 20 | HPFRCC-1% | 0.3 | 0.34 | 0.34 | 1420 | 0.8 | 78.5 | 1 | 198 | 68 | 580 |
| | 21 | HPFRCC-2% | 0.3 | 0.34 | 0.34 | 1420 | 0.8 | 157 | 2 | 198 | 68 | 580 |

M = Silica fume
C= Portland cement
W= Water
w*= Water + Superplasticizer
w/b= Water to binder ratio
b= Binder or cementitious material (cement + Micro silica)
V_f= Steel fiber volume fraction (kg and %)
A= Total of aggregate (natural + quartz sand)
w/c= Water to cement ratio
SP= Superplasticizer by weight of the binder (percent)

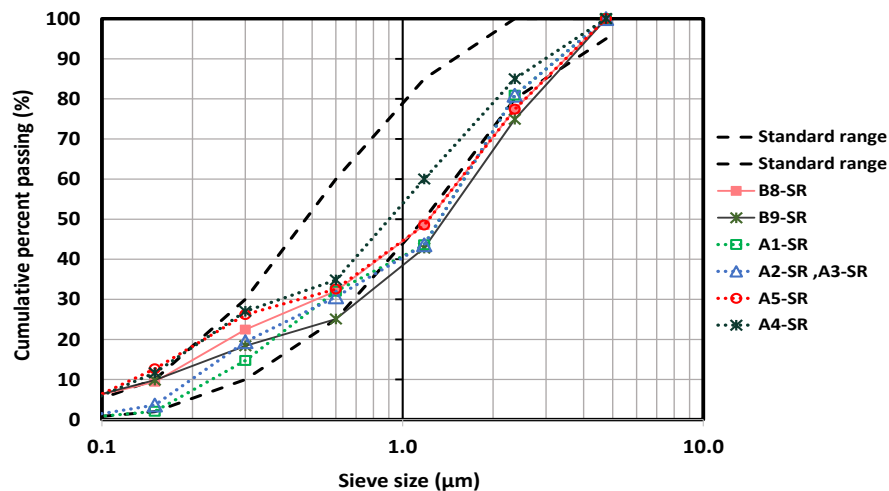
2.3. Aggregate distribution

Generally, there is a correlation between the size of aggregate particles, the water-cement ratio, the workability, and the other mechanical properties of HPFRCC. Eliminating the coarse aggregates could ensure the homogeneity of the HPFRCC

mixtures. Therefore, the maximum size of aggregates was kept at 4.75 mm. Several aggregate distributions with different sizes, types, and percentages were within the standard range of ASTM C33-93 [31] (see Fig.4.a), while others were outside the standard range for conventional concrete (see Fig.4.b).



(a) standard range.



(b) non-standard range.

Fig. 4. Aggregate distribution.

2.4. Test procedures

High-performance fiber-reinforced cementitious composites consist of high-performance concrete (HPC) and fiber-reinforced concrete (FRC). High-strength concrete demonstrates CS growth within the first few hours following production. Therefore, CS was evaluated for seven days. The CS in conventional concrete increases until 28 days, after which it will be nearly constant. Due to the remarkable increase in strength, it is also common to determine the CS at 56 and 90 days for high-strength

concrete, in addition to 28 days. It is possible to measure CS at older ages and in more significant quantities in order to make designs more cost-effective. Since HPFRCCs have high compressive strengths, it thus has the trend of increasing CS up to 56 and 90 days. In the first step, in order to characterize the CS and STS, three 100 mm × 100 mm cube specimens were created for each HPFRCC mixture at ages 7 and 28 days using the method specified in BS 1881-108 [32]. In addition, three 100 mm × 200 mm cylinder specimens were produced at ages 7 and 28 days in accordance with ASTM C496

[33]. A database containing test results on 108 concrete specimens was used to validate the developed prediction models. In the second step, 6 of 100 mm × 100 mm cube specimens and 6 of 100 mm × 200 mm cylinder specimens were made for each HPFRCC mix at the ages of 7, 28, 56, and 90 days. A total of 144 cubic and cylindrical specimens were examined in the second step to extend the proposed equation in step one. Also, the effect of fiber volume fraction and specimen age on the proposed equation was investigated. The compressive and splitting tensile tests were conducted on a universal testing machine (UTM) with a maximum load capacity of 3000kN and a continuous load rate of 0.7 MPa/s until specimen failure. The STS of the cylindrical specimen was calculated using Eq.2. The detailed test setup for the CS and STS test are presented in Fig. 5.

$$f_{sp} = \frac{2P}{\pi lD} \quad (2)$$

Where f_{sp} is STS (MPa); P is the maximum applied load indicated by the testing machine (N); l and d are the length and diameter (mm) of the cylinder specimens.



Compressive strength test Splitting tensile test
Fig. 4. The detailed test setup [4].

3. Results and discussion

In the experimental program, a total of 21 HPFRCC mixtures with five main variables, namely, the aggregate type (quartz, natural, and crushed sand), the steel fiber volume

fraction (0%, 1%, and 2%), w/b ratio (from 0.19 to 0.3), cement and silica fume amount were designed and tested. The mechanical properties of the HPFRCC series, including density, load-displacement curve, CS, STS, and cracking pattern, were investigated. Also, in step one, a relationship between CS and STS was suggested for specimens containing 1% of steel fibers volume fraction. In the second step, the proposed relationship was controlled by varying the percentages and ages of fibers.

3.1. Mechanical properties of specimen's phase 1

3.1.1. Bulk density of hardened HPFRCC

The results of the BD of hardened HPFRCC material cured at 28 days are reported in Table 6. The BD decreased with a reducing $\frac{w^*}{b}$ (or $\frac{w}{b}$) ratio, likely due to water loss. As plotted in Fig. 6, the BD of the test specimens can be correlated with the $\frac{w}{b}$ ratio (or $\frac{w^*}{b}$ ratio). New equations are proposed for estimating the BD (Eq.3 and Eq.4). In this experimental study, the maximum $\frac{w}{b}$ ratio was considered 0.3 (or $\frac{w^*}{b}$ ratio was considered 0.31). The BD was increased by 29.3% by enhancing the $\frac{w}{b}$ from 0.19% to 0.3% (or rising the $\frac{w^*}{b}$ from 0.21% to 0.31%). Overall, the density increased with $\frac{w}{b}$ (or $\frac{w^*}{b}$) ratio at a rate of $3358.4 \frac{kg}{m^3}$ (or $3169.7 \frac{kg}{m^3}$). In order to achieve lightweight HPFRCC materials, it is essential to calculate the BD and its effect on the w/c ratio. This is especially true when using HPFRCC materials in cases such as strengthening and repairing, where the designer should consider the materials to be lightweight.

$$\text{Bulk density } \left(\frac{\text{kg}}{\text{m}^3}\right) = 3358.4 \left(\frac{w}{b}\right) + 1241.5 \quad (3)$$

$$\text{Bulk density } \left(\frac{\text{kg}}{\text{m}^3}\right) = 3169.7 \left(\frac{w^*}{b}\right) + 1327.9 \quad (4)$$

3.1.2. Failure pattern of specimens

The compressive and splitting tensile failure patterns of specimens at 28 days are presented in Fig. 7. In all cases, the failure of the cubic specimens was accompanied by the appearance of multiple cracks on the sides, and pyramidal failure was never observed. Also, deep cracks were observed in the failure pattern of the cylindrical specimens, while the number of fine cracks grew and the specimen did not split completely.

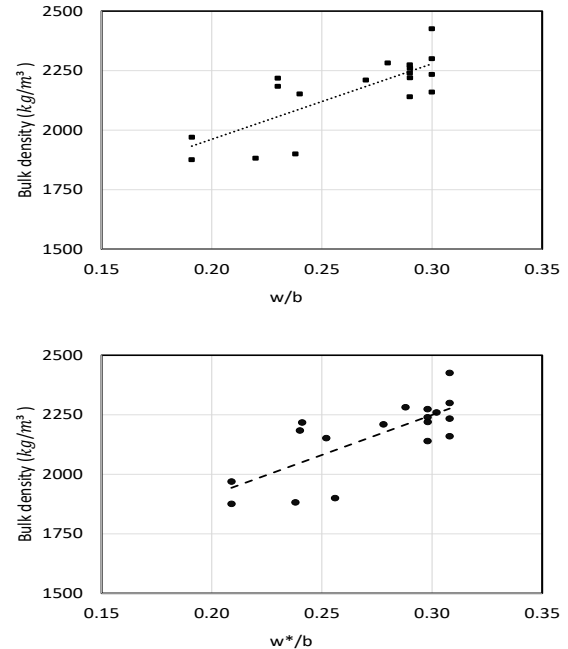


Fig. 6. BD $\frac{w}{b}$ ($\frac{w^*}{b}$) ratio curve.

Table 6. Mix proportions for HPCRCC (data for 1 m³).

| Mix name | Measured Density | BD (kg/m ³) | | | |
|----------|------------------|-------------------------|------------|-------|--------------|
| | | Eq. 4 | Error-Eq.3 | Eq. 5 | Error- Eq. 4 |
| A1-SR | 2426 | 2276 | 6/2 | 2279 | 6/1 |
| A2-SR | 2160 | 2276 | -5/4 | 2279 | -5/5 |
| A3-SR | 1900 | 2101 | -10/6 | 2082 | -9/6 |
| A4-SR | 2282 | 2209 | 3/2 | 2215 | 2/9 |
| A5-SR | 2234 | 2276 | -1/9 | 2279 | -2/0 |
| A6-NSR | 2300 | 2276 | 1/0 | 2279 | 0/9 |
| A7-NSR | 2240 | 2242 | -0/1 | 2247 | -0/3 |
| A8-NSR | 2274 | 2242 | 1/4 | 2247 | 1/2 |
| A9-NSR | 2140 | 2242 | -4/8 | 2247 | -5/0 |
| B1-NSR | 1970 | 1943 | 1/3 | 1933 | 1/9 |
| B2-NSR | 1882 | 2041 | -8/4 | 2025 | -7/6 |
| B3-NSR | 2220 | 2242 | -1/0 | 2247 | -1/2 |
| B-4-NSR | 1876 | 1943 | -3/6 | 1933 | -3/1 |
| B5-NSR | 2152 | 2088 | 3/0 | 2089 | 2/9 |
| B6-NSR | 2210 | 2175 | 1/6 | 2184 | 1/2 |
| B7-NSR | 2184 | 2048 | 6/2 | 2057 | 5/8 |
| B8-SR | 2218 | 2051 | 7/5 | 2057 | 7/3 |
| B9-SR | 2260 | 2256 | 0/2 | 2247 | 0/6 |

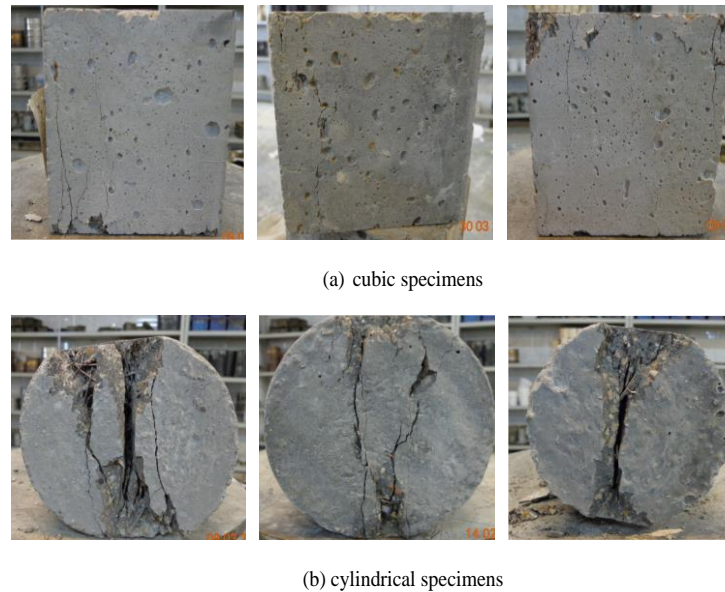


Fig. 7. Failure pattern of step one at 28 day.

3.1.3. CS and STS strength

The average CS and STS of the 1%-HPFRCC at 7 and 28 days are reported in Table 7. Each result of the tensile strength test was the average value of the three specimens from step one. In accordance with a result, adding fibers to the mixing design increased CS due to the prevention of crack propagation but decreased CS due to an increase in the amount of air entrained. Therefore, the effects of fiber addition on CS are minimal. However, the addition of fibers significantly increased the specimen's fracture force.

In this section, different variables, such as w/b ratio, aggregate distribution, aggregate type (quartz, natural, and crushed sand), and weight, were evaluated for their effects on the CS and STS. Two identical mixing designs, A2-SR and A3-SR, with the exception of the superplasticizer, revealed that increasing the superplasticizer by 1% significantly decreased CS and STS by roughly 100 and 66%, respectively. By substituting crushed sand with natural sand,

the CS and STS of HPFRCC increased significantly (approximately 25% and 42%, respectively).

Table 7. CS and STS of specimen's step one.

| Specimen's name | (Cylinder 10×20 mm) | | (Cube 10×10 mm) | |
|-----------------|---------------------|-------|-----------------|-------|
| | Days | | Days | |
| | 7 | 28 | 7 | 28 |
| A1-SR | 7.7 | 9.4 | 66.8 | 89.0 |
| A2-SR | 5.70 | 8.30 | 39.30 | 61.70 |
| A3-SR | 3.10 | 5.00 | 18.00 | 30.00 |
| A4-SR | 5.70 | 7.00 | 44.20 | 68.50 |
| A5-SR | 6.00 | 10.00 | 55.00 | 85.00 |
| A6-NSR | 6.00 | 9.40 | 53.00 | 76.00 |
| A7-NSR | 5.30 | 8.60 | 42.00 | 62.00 |
| A8-NSR | 6.10 | 9.00 | 51.00 | 68.00 |
| A9-NSR | 5.00 | 6.50 | 38.00 | 50.00 |
| B1-NSR | 5.70 | 7.90 | 42.00 | 67.00 |
| B2-NSR | 4.00 | 5.60 | 27.00 | 38.00 |
| B3-NSR | 3.90 | 5.00 | 26.00 | 37.00 |
| B4-NSR | 5.70 | 7.30 | 41.00 | 66.00 |
| B5-NSR | 6.30 | 7.60 | 53.00 | 73.00 |
| B6-NSR | 6.10 | 8.90 | 52.00 | 83.00 |
| B7-NSR | 6.70 | 8.00 | 57.00 | 85.00 |
| B8-SR | 6.30 | 9.00 | 53.00 | 81.00 |
| B9-SR | 6.80 | 8.60 | 57.00 | 84.00 |

According to the data, the type of fine sand (smaller than 0.5 mm) was another critical factor for CS and STS changes, as quartz sand in A2-SR increased CS and STS by almost 44.2% and 13% compared to A1-SR with normal sand, respectively. The next factor that affected CS and STS was the quantity of fine aggregate. A nearly 20% increase in fine aggregate between A1-SR and A5-SR mix proportion reduced the CS by 5%; however, there was a 6% increase in the STS, which could be attributed to improved fiber and mortar cohesion.

3.1.4. The proposed equation for estimating the STS, f_{sp}

Nonlinear regression analysis (NLR) (curve fitting method) is a technique used to propose

a relationship for estimating the STS of HPFRCC materials from the CS. In the discussion, a simple equation model (Eq6) was employed in which the tensile strength of the HPFRCC material is proportional to the square root of their CS. This model is one of the most widely used analytical models.

$$f_{sp} = \alpha \times f_c^\beta \quad (6)$$

The curve of the ratio of STS to CS versus CS is given in Fig 8. This demonstrates the ratio of STS to CS, which is dependent on the CS and decreases as CS increases. The current study indicated that increasing the CS from 15 to 85 decreased the ratio of STS to CS from 0.21 to 0.1.

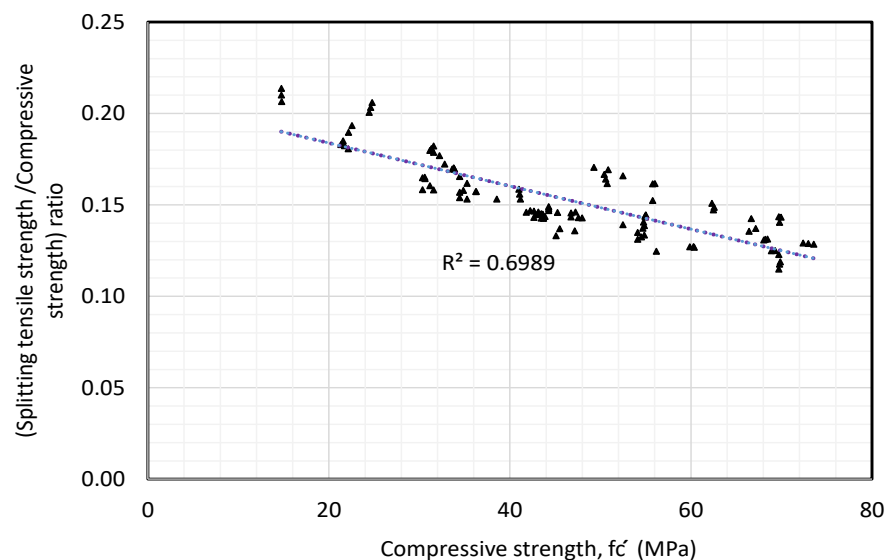


Fig. 8. The curve of the ratio of STS to CS versus CS in step one.

Previous research on proposing an equation for estimating the STS of fiberless concrete indicated that CS, curing time, aggregate type, specimen size, water-to-cement ratio, and the testing method are crucial parameters for the proposed relationship [34]. Moreover, important parameters such as fiber types, fiber aspect ratio, fiber content, and fiber length can impact the tensile strength of

FRCs. In addition, the number of specimens tested is a critical parameter because it provides stronger statistical support for the proposed relationship. Using more extensive statistical data enables the proposed relationship to be applied to a wider variety of mixing designs. However, this study proposed equations for a relatively small number of specimens comprised of HPFRCC

materials and for their CS only. Therefore, additional research is warranted to investigate the effect of other parameters mentioned above. The experimental results of f_{sp} and f_c are plotted in Fig.9, and the following new equation is proposed for estimating the STS (Eq.7):

$$f_{sp} = 0.498 \times f_c^{0.68} \quad (7)$$

In statistics, the Coefficient of Determination (COD) allows us to determine the extent to which a reliable model can predict, which

was calculated at 0.94 for Eq.7. As shown in Fig.10, the STS predictions based on Eq.7 agreed favorably with the test results of the present study. The prediction errors run below $\pm 15\%$ (Eq.8).

$$PE = 100 * \frac{PV - MV}{MV} \quad (8)$$

PE: Prediction error
 PV: predicted value
 MV: measured value

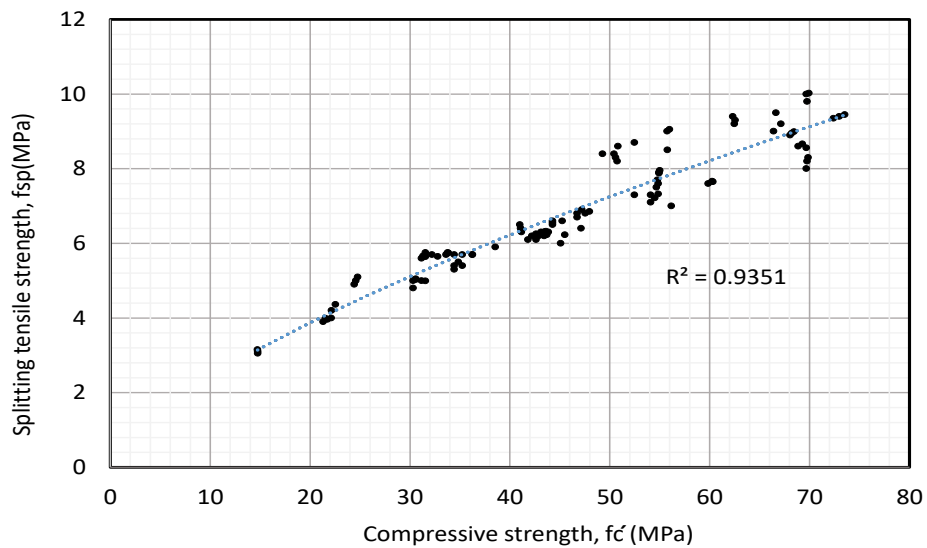


Fig. 9. The CS versus STS curve.

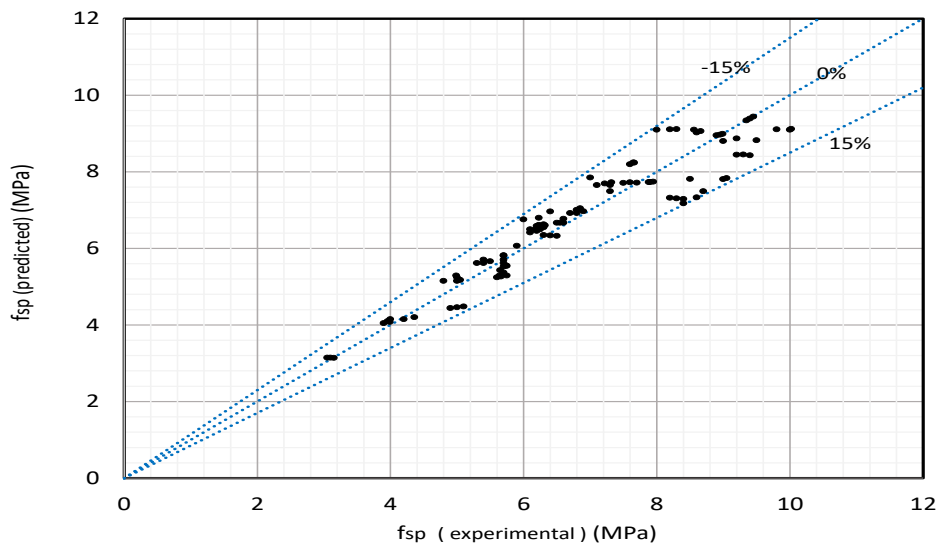


Fig. 10. The predicted error between the experimental and predicted value of STS.

Fig11 depicts the STS prediction models proposed by other researchers as well as the models developed in this study. The conditions under which the model/equation was developed (e.g., range of f_c) were factored into the calculation of the suggested models so that the predicted relationship could be compared to the relationships provided by other researchers. Based on the statistical analysis, the predicted values of STS differed from the experimental values for all the tested models. Among the different predicted models, the function proposed by Xu and Shi provides marginally better fits (i.e., for HPRCC materials with 1% volume fraction steel fiber) than the other provided models [18]. The discrepancy between the previously proposed function and the

equation proposed in this study is due to the different types of concrete or cementitious mortar. Since the tensile strength of ordinary concrete is relatively low, fiber-reinforced concrete does not exhibit strain hardening behavior, and the tensile strength of fiber-reinforced concrete is lower than that of high-performance fiber-reinforced cementitious composite. Due to the small number of specimens and using 21 roughly similar mixing schemes, it was difficult to predict the relationship for a broader range of fiber-reinforced concrete specimens. Therefore, further research, including numerical and experimental studies, is required to provide a more comprehensive relationship.

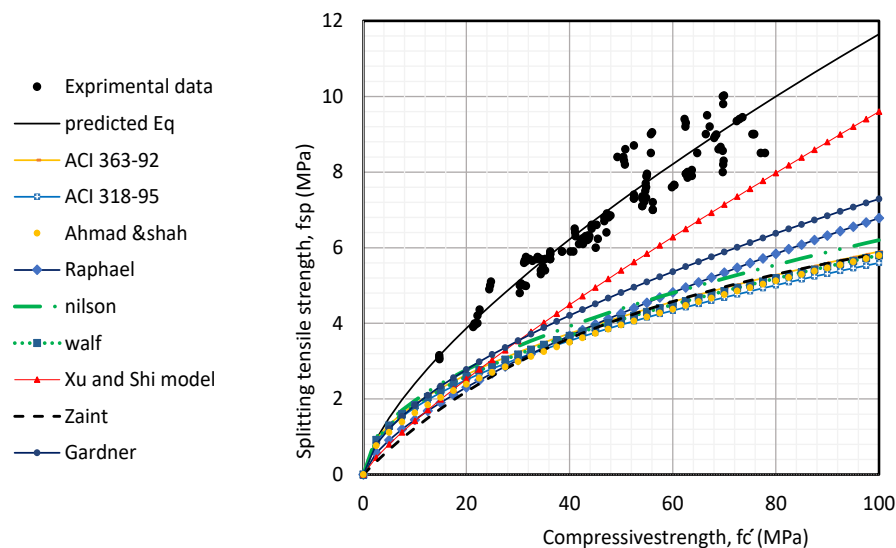


Fig. 11. Comparison of the predicted Eq and the other Eq.

3.2. Mechanical properties of specimen's phase two

3.2.1. Failure pattern of specimens

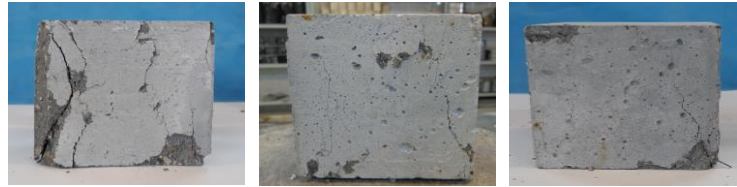
Fig.12-a depicts the compressive failure patterns of cubic specimens at 7 and 28 days. It varies with the volume fraction of steel fibers. Also, Fig.12-b displays the tensile failure patterns of cylindrical specimens at 7

and 28 days. The specimens without any steel fiber (HPRCC-0%) can be seen to be wholly divided into two parts. The fraction of steel fiber enhanced failure patterns. The typical fracture surfaces with different steel fiber volume fractions are shown in Fig.13. The fracture surface of specimens without steel fiber was smooth, whereas the fracture surface of specimens with steel fiber was rough.



(a) HPFRCC-0% (b) HPFRCC-1% (c) HPFRCC-2%

Failure pattern of cubic specimens at 7 days.



(a) HPFRCC-2% (b) HPFRCC-1% (c) HPFRCC-0%

Failure pattern of cubic specimens at 28 days.

(a) Cubic specimens.



(a) HPFRCC-0% (b) HPFRCC-1% (c) HPFRCC-2%

Failure pattern of cylindrical specimens at 7 days



(a) HPFRCC-0% (b) HPFRCC-1% (c) HPFRCC-2%

Failure pattern of cylindrical specimens at 28 days

(b) Cylindrical specimens

Fig. 12. Failure pattern of specimens.



(a) without fibers.



(b) with fibers.

Fig. 13. Comparison of the fracture plane of specimens.

3.2.2. CS and STS of specimen

Table 8 summarizes the average CS and STS of the test specimens used in this experiment's second phase. The addition of fibers to the cement composite mixture had a negligible effect on the CS but a significant effect on the STS determined by the splitting tensile test. At 28 days, for instance, adding 1% and 2% fibers increased the tensile strength by 54% and 95%, respectively, compared to specimens without fibers.

Table 8. Average compressive and tensile strength of the specimen's step two.

| Specimen's name | | Days | | | |
|-----------------|-----------|------|------|------|------|
| | | 7 | 28 | 56 | 90 |
| CS | HPCC-0% | 49.9 | 69.8 | 73.0 | 78.5 |
| | HPFRCC-1% | 47.0 | 64.0 | 77.7 | 92.0 |
| | HPFRCC-2% | 51.3 | 72.0 | 77.0 | 93.0 |
| STS | HPCC-0% | 3.1 | 4.8 | 5.2 | 5.8 |
| | HPFRCC-1% | 5.9 | 7.4 | 7.9 | 9.0 |
| | HPFRCC-2% | 6.2 | 9.4 | 10.4 | 11.1 |

3.2.3. Investigation of the relationship of the specimen

3.2.3.1. Relationship between STS and CS

The test results of the second step demonstrated that the addition of steel fibers soared the STS of HPFRCC specimens. Fig.14 depicts the curve STS to CS ratio versus CS drawn for specimens with 0%, 1%, and 2% fibers. This curve illustrates that as the CS increases, the ratio of STS to CS decreases for specimens containing fibers, but remains nearly constant for specimens lacking fibers. Therefore, in consonance with Fig.15, the proposed equation in the first step can be utilized with a 20% error for HPFRCC containing 2% fiber (the predicted error calculated with Eq.8 in the 3.1.4 section). In contrast, the predicted error for the HPFRCC without fiber ranged from 40% to 100%.

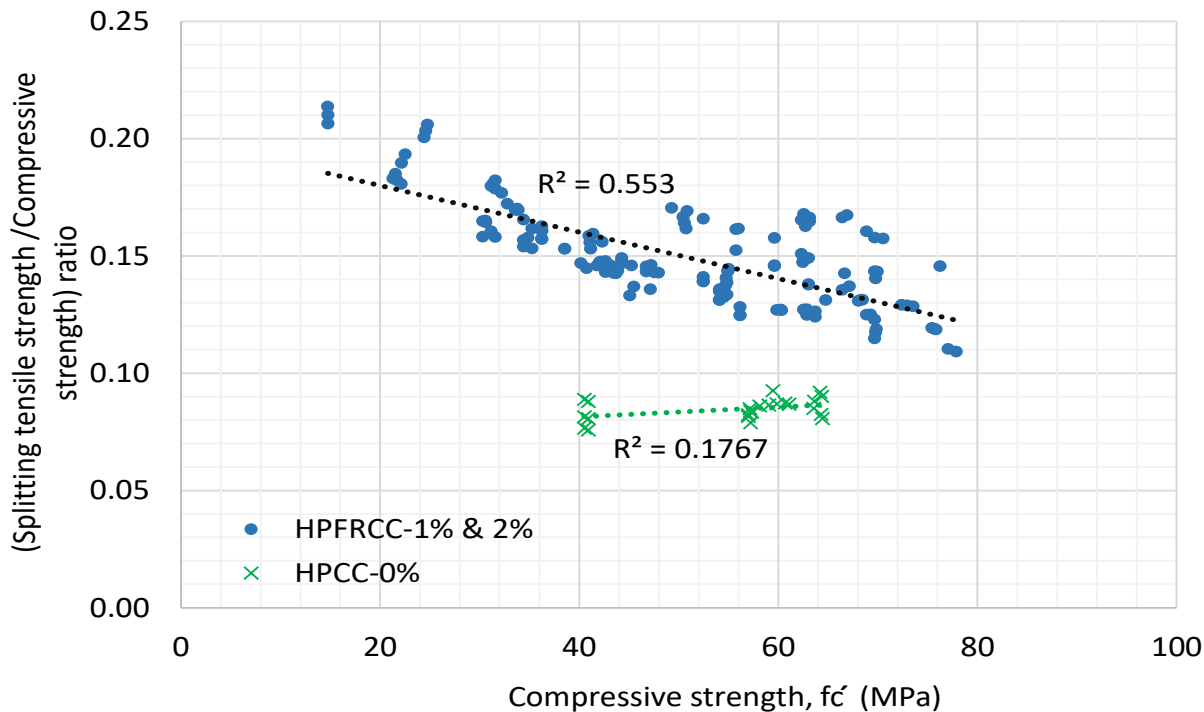


Fig. 14. Comparison of the STS to CS ratio versus CS.

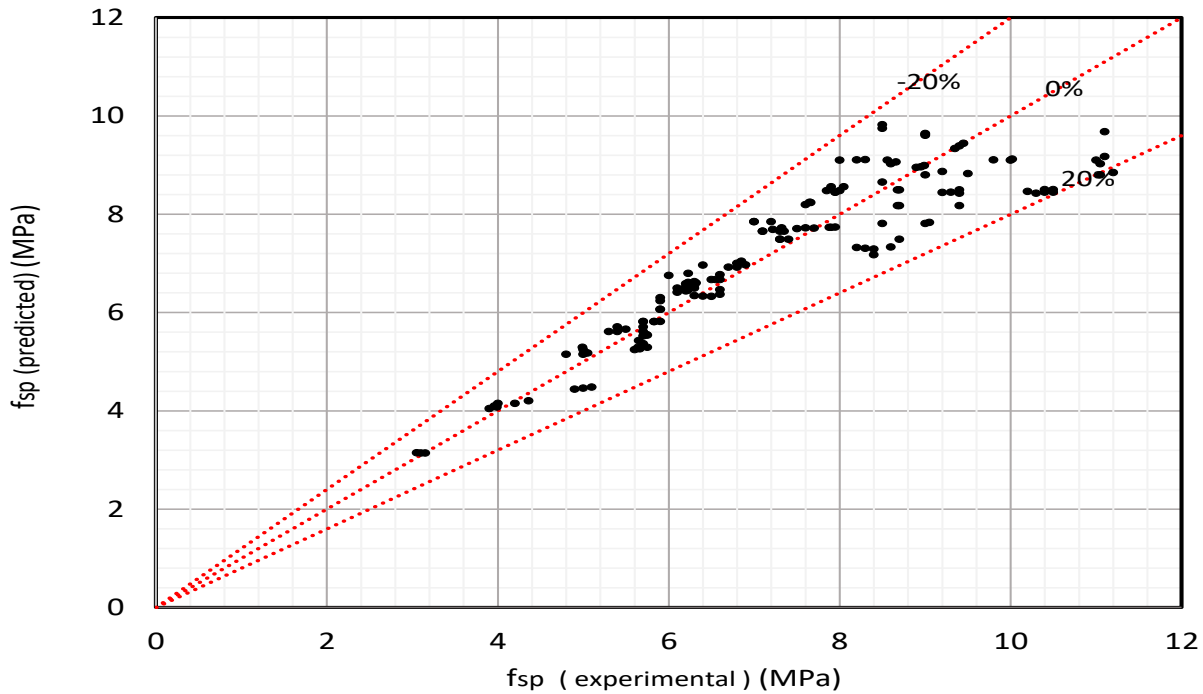


Fig. 15. Predicted error for all of the specimens with fiber (1% and 2%).

On the other hand, comparing the fiber-free specimens with models proposed by other researchers, as shown in Fig.16, revealed that a good approximation can be used to calculate the STS for the fiber-free specimens. In this respect, the following relationships can be stated: Gardner [26] and Raphael's [21] model for determining the tensile strength of specimens with CS greater than 60 MPa and Ahmad & Shah's [15] and Zaint's [24] models for determining the STS of specimens with CS less than 45 MPa.

3.2.3.2. Relationship between CS and age of the specimen

The CS of concrete increases over time; for concrete cured to the age of testing at 21°C and made by type I cement, ACI 209.2R-08 [35] recommends Eq.9.

$$\hat{f}_c(t) = \hat{f}_{c,28} \left(\frac{t}{4 + 0.85t} \right) \quad (9)$$

Where t is the time after concrete casting (day), $f'_c(t)$ and $f'_{c, 28}$ are the CS of the

concrete after t day and 28 days, respectively. Fig.17 displays the experimental data for the reference, HPFRCC-1%, and HPFRCC-2% specimens, as well as the proposed Eq.9. Calculating the CS at ages older than 28 days using Eq.9 with an error of less than 6% is permitted based on the results. The slight difference between the experimental values and the relationship can be explained by the presence of steel fibers and the variation in cement type.

Tensile and CS values were affected by variables such as the type of fiber (length and diameter of aspect ratio), fiber volume fraction, and age of the specimen. Consequently, providing a more precise relationship that encompasses all the parameters was a more difficult task that could be accomplished using a neural network method. Therefore, future research articles must consider these parameters.

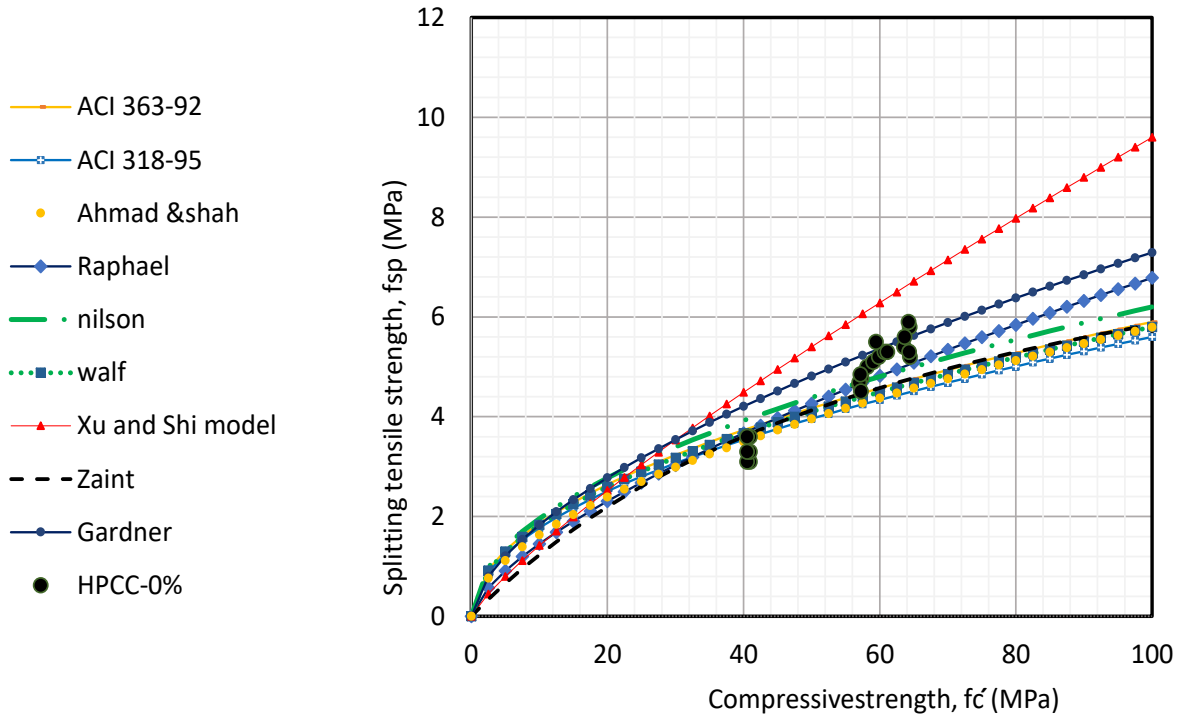


Fig. 16. Comparison of the experimental data of fiber free HPCFRCC and the other equations.

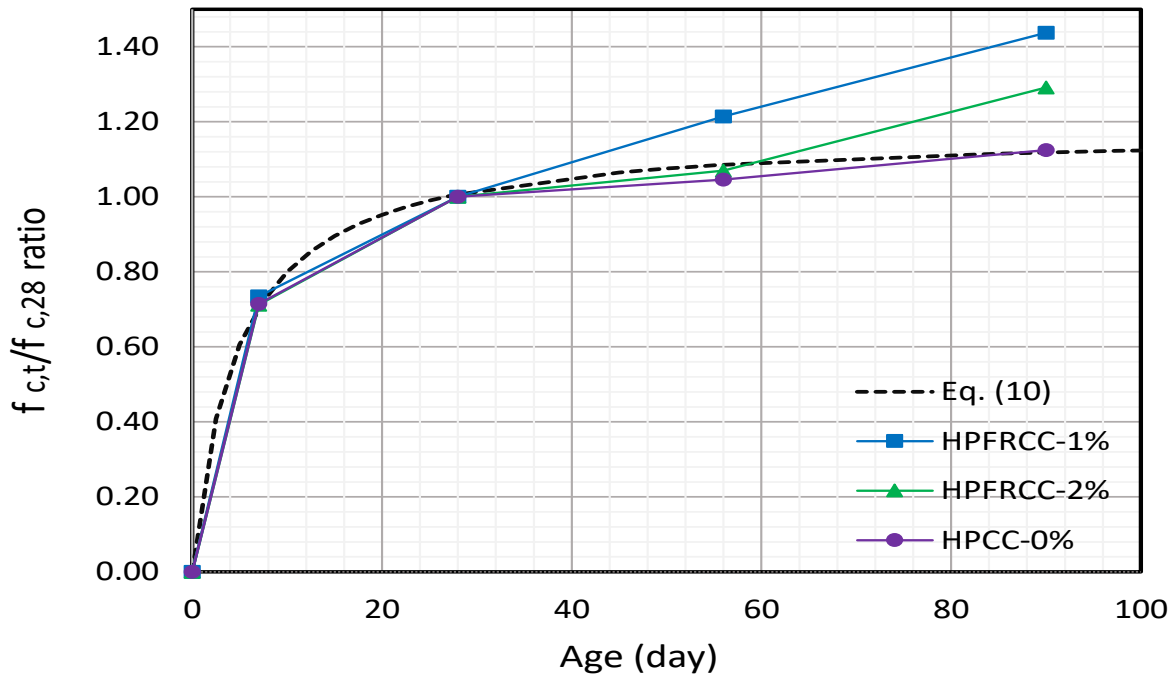


Fig. 17. The ratio of CS of specimens at different ages to 28 days versus days.

4. Conclusions

Based on the experimental result of the HPFRCC in this study, the maximum $\frac{w}{b}$ ratio, which was considered 0.3, the following conclusions were drawn:

- The BD was grown by 29.3% by increasing the $\frac{w}{b}$ from 0.19% to 0.3% (or rising the $\frac{w^*}{b}$ from 0.21% to 0.31%), likely due to water loss. New equations for estimating the bulk density (BD) are proposed. Overall, the density increased with $\frac{w}{b}$ (or $\frac{w^*}{b}$) ratio at a rate of 3358.41 $\frac{\text{kg}}{\text{m}^3}$ (or 3169.7 $\frac{\text{kg}}{\text{m}^3}$).
- Patterns of failure for specimens devoid of steel fiber (HPCC-0%) were completely divided into two parts. The fraction of steel fiber had enhanced failure patterns. The fracture surface of specimens without steel fiber was smooth, whereas the fracture surface of specimens with steel fiber was rough.
- Adding fibers to the cement composite mixture had a negligible effect on the CS but a significant effect on the STS determined by the splitting tensile test. At 28 days, for instance, adding 1% and 2% fibers increased the tensile strength by 54% and 95%, respectively, compared to specimens without fibers.
- The relationship between STS and CS of HPFRCC containing 1% steel fibers was proposed with prediction errors running below $\pm 15\%$.
- The proposed equation of HPFRCC with 1% steel fiber can be used with a 20% error for specimens containing 2% fiber, while the predicted error ranges from 40% to 100% for the specimens without fiber.

- With good approximation, the equations proposed by other researchers, primarily the functions provided for high-strength concrete, can be used to calculate the STS for fiber-free specimens.
- In HPFRCC materials, the experimental equation can be used to calculate CS based on sample age and CS 28 with an error of less than 6% (ACI 209-08 [35]). The slight difference between the experimental values and the relationship can be attributed to the presence of steel fibers and the varying number of days the specimens were cured in water.

Acknowledgment

The authors would like to express their gratitude to members of the concrete technology laboratory of Semnan University for their helpful assistance throughout the experimental work.

Funding

We would like to clarify that this research received no external funding from any organization or agency. All expenses related to the experimental work, data analysis, and manuscript preparation were covered by the authors themselves. We acknowledge that this research was conducted independently and without the influence of any external funding source.

Conflicts of interest

One of the authors of the article (Prof. Ali Kheyroddin) is the "Editor-in-Chief" of the journal. Based on the journal policy, this author was completely excluded from any review process of this article and the review process of this article.

Authors contribution statement

Mahdieh Sabbaghian: Data curation, Formal analysis, Funding acquisition, Investigation, Methodology, Software, Validation, Visualization, writing – original draft, Writing – review & editing.

Ali Kheyroddin: Data curation, Formal analysis, Funding acquisition, Investigation, Methodology, Project administration, Resources, Supervision, Validation, Visualization, Writing – review & editing.

References

- [1] Němeček J, Kabele P, Bittnar Z. Nanoindentation based assessment of micro-mechanical properties of fiber reinforced cementitious composite. 6th Int RILEM Symp Fibre-Reinforced Concr (FRC 2004:401–10.
- [2] Naaman AE. High performance fiber reinforced cement composites: classification and applications. CBM-CI Int Work Karachi, Pakistan 2009;1:389–401. <https://doi.org/978-969-8620-06-6>.
- [3] Daneshvar K, Moradi MJ, Amooie M, Chen S, Mahdavi G, Hariri-Ardebili MA. Response of low-percentage FRC slabs under impact loading: Experimental, numerical, and soft computing methods. Structures 2020;27:975–88. <https://doi.org/10.1016/J.ISTRUC.2020.06.005>.
- [4] Sabbaghian M, Kheyroddin A. Flexural strengthening of RC one way slabs with high-performance fiber-reinforced cementitious composite laminates using steel and GFRP bar. Eng Struct 2020;221:111106. <https://doi.org/10.1016/J.ENGSTRUCT.2020.111106>.
- [5] Ghods A, Sharbatdar MK. An investigation on the behavior of two fixed end beams cast with HPFRCC composite. Case Stud Constr Mater 2020;13:e00466. <https://doi.org/10.1016/J.CSCM.2020.E00466>.
- [6] Moolaei S, Sharbatdar MK, Kheyroddin A. Experimental evaluation of flexural behavior of HPFRCC beams reinforced with hybrid steel and GFRP bars. Compos Struct 2021;275:114503. <https://doi.org/10.1016/J.COMPSTRUCT.2021.114503>.
- [7] Ehsani R, Sharbatdar MK, Kheyroddin A. Ductility and moment redistribution capacity of two-span RC beams. Mag Civ Eng 2019;90:104–18. <https://doi.org/10.18720/MCE.90.10>.
- [8] Parsa E, Sharbatdar MK, Kheyroddin A. Investigation of the Flexural Behavior of RC Frames Strengthened with HPFRCC Subjected to Lateral Loads. Iran J Sci Technol Trans Civ Eng 2018 432 2018;43:231–40. <https://doi.org/10.1007/S40996-018-0133-0>.
- [9] Sabbaghian M, Kheyroddin A. Effect of grading and superplasticizer content on mechanical properties of High-performance fiber reinforced cement composites (HPFRCC). 11th Natl. Congr. Civ. Eng. Shiraz Univ. Shiraz, Iran, 2019.
- [10] Sabbaghian M, Kheyroddin A. Experimental Investigation of the Effect of Fiber on Mechanical and the Age Properties of High-Performance Fiber Reinforced Cement Composites. Concr Res Q J 2020;12:53–68. <https://doi.org/10.22124/JCR.2019.11889.1321>.
- [11] Sabbaghian M, Kheyroddin A. Experimental investigation of shear behavior of one-way reinforced slabs with high-performance fiber-reinforced cementitious composite laminates.

- Amirkabir J Civ Eng 2022;53:919–22. <https://doi.org/10.22060/CEEJ.2020.18138.6778>.
- [12] Sabbaghian M, Kheyroddin A. The relationship between compressive strength and splitting tensile strength of HPFRCC . 3rd Int. Conf. Civ. Eng. Archit. Urban Manag. Iran, 2020.
- [13] Ramadoss P, Nagamani K. Tensile strength and durability characteristics of high-performance fiber reinforced concrete. *Rabian J Sci Eng* 2008;33:307–19.
- [14] Yazıcı Ş, İnan G, Tabak V. Effect of aspect ratio and volume fraction of steel fiber on the mechanical properties of SFRC. *Constr Build Mater* 2007;21:1250–3. <https://doi.org/10.1016/j.conbuildmat.2006.05.025>.
- [15] Shah SP, Ahmad SH. Structural properties of high-strength concrete and its implications for prestressed concrete. *PCI J* 1985;30:92-119.
- [16] Nataraja, M., Dhang, N. & Gupta A. Splitting tensile strength of steel fiber-reinforced concrete. *Indian Concr J* 2001;75.
- [17] Ramadoss P. Studies on high performance steel fiber reinforced concrete under static and impact loads. Anna univ, 2007.
- [18] Xu BW, Shi HS. Correlations among mechanical properties of steel fiber reinforced concrete. *Constr Build Mater* 2009;23:3468–74. <https://doi.org/10.1016/j.conbuildmat.2009.08.017>.
- [19] American Concrete Institute. State of the art report on high-strength concrete-ACI363R-1992. 2004.
- [20] American Concrete Institute. Building code requirements for structural concrete and commentary-ACI318-1995 and ACI318R-1995. 2004.
- [21] Raphael JM. tensile strength of concrete. *J Am Concr Inst* 1984;81:158–65.
- [22] Nilson AH. Design implication of current research on high- strength concrete. *Spec Publ* 1985:85–118.
- [23] Wafa, F. F., and Ashour SA. Mechanical properties of high- strength fiber reinforced concrete. *ACI Mater J* 1992;89:449–455.
- [24] M.F.M. Zain, H.B. Mahmud, A. Ilham MF. Prediction of splitting tensile strength of high-performance concrete. *Cem Concr Res* 2002;32:1251–8.
- [25] Perumal R. Correlation of compressive strength and other engineering properties of high-performance steel Fiber–Reinforced Concrete. *J Mater Civ Eng* 2015;27:04014114. [https://doi.org/10.1061/\(ASCE\)MT.1943-5533.0001050](https://doi.org/10.1061/(ASCE)MT.1943-5533.0001050).
- [26] Gardner NJ, Sau PL, Cheung MS. Strength development and durability of concretes cast and cured at 0 C. *Mater J* 1988;85:529–36.
- [27] ASTM C494/C494M. Standard Specification for Chemical Admixtures for Concrete 1. 2004.
- [28] ASTM A820. Standard Specification for Steel Fibers for Fiber-Reinforced Concrete. West Conshohocken, PA, USA: 2011.
- [29] ASTM C143-15. Standard test method for slump of hydraulic-cement concrete. West Conshohocken, PA, USA: 2015.
- [30] ASTM C31/C31M. Standard Test Practice for Making and Curing Concrete Test Specimens in the Field. West Conshohocken, PA, USA: 2021.
- [31] ASTM C33-93. Standard Specification for Concrete Aggregates. West

Conshohocken, PA, USA: 2018.

- [32] BS1881-108. Testing concrete- Part 108. Method for making test cubes from fresh concrete. 1993.
- [33] ASTM C496/C496M. Standard test method for splitting tensile strength of cylindrical concrete specimens. West Conshohocken, PA, USA: 2004.
- [34] Ramesh K, Seshu DR, Prabhakar M. Constitutive behaviour of confined fibre reinforced concrete under axial compression. *Cem Concr Compos* 2003;25:343–50.
[https://doi.org/10.1016/S0958-9465\(02\)00051-3](https://doi.org/10.1016/S0958-9465(02)00051-3).
- [35] ACI 209.2R-08. Guide for Modeling and Calculating Shrinkage and Creep in Hardened Concrete. 2008.